



Characteristics of Photon–Plasmon Coupling in Uniaxial Chiral Filled Slab Waveguide Bounded by Graphene Layers

Ahmed Mahal¹ · Hussein H. Abdulghani² · Raad A. Khamis³ · Yazeed M. Asiri⁴ · Mohammed A. Amin⁴ · Majid S. Jabir² · Hasan Majdi⁵ · Fahad M. Almutairi⁶ · Adel Ashour⁷ · Mohamed Shaban^{7,8} · Laiba⁹

Received: 27 April 2024 / Accepted: 6 June 2024

© The Author(s), under exclusive licence to Springer Science+Business Media, LLC, part of Springer Nature 2024, corrected publication 2024

Abstract

In this manuscript, characteristics of photon–plasmon coupling in uniaxial chiral-filled slab waveguide bounded by graphene layers are analyzed. We have explored some novel features of surface plasmon polaritons (SPPs) owing to the interaction between uniaxial chiral and graphene layers. The influence of graphene's features and chirality on the SPPs behavior are examined. The tunability of proposed waveguide structure is shown to study the effect of chirality, chemical potential, relaxation time, and separation distance between the plates on the normalized propagation constant versus operating frequency. Furthermore, the influence of chemical potential and separation distance between graphene layers on attenuation are also analyzed. This integration of graphene layers provides an extra degree of freedom to the fabricate graphene-based nanophotonic devices in the optics sector.

Introduction

Speed and data transmission rates are reaching their fundamental limits for semiconductor devices and modern electronic integrated devices. One of the most promising

solutions might be to use light in electronic circuits rather than electrons. Due to diffraction limit of light, it may not be feasible to fabricate nanophotonic devices if the size of the device is smaller than the wavelength of light. An effective method for circumventing the diffraction limit is the use of surface plasmon polaritons (SPPs) and electromagnetic waves (dielectric medium) coupled to charge oscillations (metal). SPPs can be localized in nanoscale regions with wavelengths substantially shorter than light wavelengths [1–4]. At metal–dielectric interface, electromagnetic surface wave shows attenuation as it moves away from the interface. Due to these extraordinary features, SPPs play a vital role in enabling photonic devices and signal processing devices to be manufactured at a sub-wavelength scale [5]. Terahertz (THz) radiation has been attracting increasing interest over the past few decades. By virtue of the unique nature of THz waves, several novel applications may be enabled, including THz spectroscopy, sensing, imaging, and communication [6–11]. There are several plasmonic materials with common wavelengths such as Au, Ag, and Al that can produce SPPs at wavelengths below the mid-infrared (IR) region of the electromagnetic spectrum. In plasmonics sector, it is very necessary to confine the THz EM wave to a scale of a few nanometers to achieve the desired results. In contrast, metals do not have the capacity to effectively support surface waves at microwave and THz frequencies [12, 13]. Graphene, ultrathin, two-dimensional, hexagonal structure with its honeycomb lattice has recently received a

✉ Laiba
laiba222rana@gmail.com; physicsscholar232@gmail.com

¹ Department of Medical Biochemical Analysis, College of Health Technology, Cihan University-Erbil, Erbil, Kurdistan Region, Iraq

² Department of Applied Sciences, University of Technology, Baghdad, Iraq

³ College of Sciences, Uruk University, Baghdad, Iraq

⁴ Department of Chemistry, College of Science, Taif University, P.O. Box 11099, Taif 21944, Saudi Arabia

⁵ Department of Chemical Engineering and Petroleum Industries, Al-Mustaqbal University College, Babylon 51001, Iraq

⁶ Biochemistry Department, Faculty of Science, University of Tabuk, Tabuk 71491, Saudi Arabia

⁷ Department of Physics, Faculty of Science, Islamic University of Madinah, Madinah 42351, Saudi Arabia

⁸ Nanophotonics and Applications (NPA) Lab, Physics Department, Faculty of Science, Beni-Suef University, Beni-Suef 62514, Egypt

⁹ Department of Mathematics, Government College University Faisalabad, Faisalabad, Pakistan

considerable amount of attention from the academic community due to its remarkable electronic transport properties and potential applications in the optics sector [14]. In comparison to other plasmonic materials, these properties are very useful for the advancement of sensor technology. In addition to high carrier mobility, rapid photoresponse, and a wide range of optical spectrum coverage from the ultraviolet to the THz ranges [15]. A new platform for terahertz (THz) plasmonics has emerged thanks to graphene’s unique electronic and optical traits [16]. The charge carriers in graphene are highly unusual response and behave as Dirac fermions [17]. This peculiar trait has a profound influence on the energy spectrum of landau levels produced in the presence of a magnetic field. Electrical gating allows for tuning graphene’s absorption of incident light [18–21]. Furthermore, graphene exhibits extraordinary thermal conductivity (5000 w/m⁻¹ K⁻¹) which is very useful in fabricating and designing nanophotonic devices [22]. Additionally, electrostatic gating or magnetostatic gating can be used to tune graphene’s transport properties and electrical conductivity [23]. Variety of methods were investigated to explore the characteristics of SPPs by several authors [24–29]. In this context, Guangcan Mi and Vien Van presented the numerical analysis of SPPs at chiral-metal planar interface to analyze the effective mode index, propagation length, and fields profile for chiral sensing applications [30]. Heydari and Samiei numerically investigate the SPP characteristics at metal-chiral-metal parallel plate waveguide structure to fabricate nanophotonic devices. Umair et al. analyzed the numerical analysis of EM surface waves at chiral-plasma interface [31]. In the case of an isotropic chiral material, the degree of chirality can only be controlled to a very limited extent. To overcome this challenge, uniaxial chiral (UAC) material is used. UAC material, in contrast to other optical materials, possess more constitutive parameters, as explained in Eq. (1), providing a degree of freedom in controlling SPPs. A further characteristic of UAC material is that it exhibits both positive and negative permittivity at the same time. In comparison with conventional optical materials, UAC material offer the potential for new advances in surface-wave research and development due to the controllable nonhomogeneity of the material. The literature survey motivated us to study the characteristics of photon–plasmon coupling in uniaxial chiral-filled slab waveguide bounded by graphene layers.

Methodology

Figure 1 presents the schematic of graphene-UAC-graphene waveguide structure. UAC is sandwiched between graphene layers. ϵ_t, μ_t , and ϵ_z, μ_z are components of UAC material. Consider SPP wave propagating along z-axis. The monolayer conductivity of graphene is characterized by Kubo formalism.

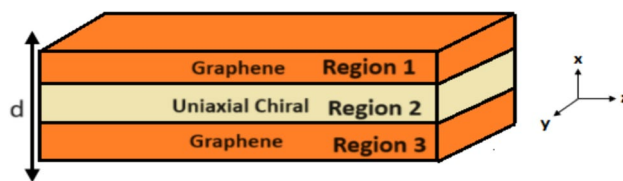


Fig. 1 Uniaxial chiral sandwiched slab waveguide surrounded by graphene layers

For region 1, EM fields are given below:

$$E_{z1} = A_1(e^{-\alpha_{m1}x}) \tag{1}$$

$$H_{z1} = A_2(e^{-\alpha_{m1}x}) \tag{2}$$

$$E_{y1} = \frac{i\omega\mu_0}{\alpha_{m1}} A_2(e^{-\alpha_{m1}x}) \tag{3}$$

$$H_{y1} = -\frac{i\omega\epsilon_0}{\alpha_{m1}} A_1(e^{-\alpha_{m1}x}) \tag{4}$$

where ω, μ_0 , and ϵ_0 represent the operating frequency, permeability, and permittivity of free space.

For region 2, EM fields are:

For UAC, the constitutive relations are given below:

$$\mathbf{D} = [\epsilon_t \hat{\mathbf{I}}_t + \epsilon_z \hat{e}_z \hat{e}_z] \cdot \mathbf{E} - j\xi \sqrt{\mu_0 \epsilon_0} \hat{e}_z \hat{e}_z \cdot \mathbf{H} \tag{5}$$

$$\mathbf{B} = [\mu_t \hat{\mathbf{I}}_t + \mu_z \hat{e}_z \hat{e}_z] \cdot \mathbf{H} - j\xi \sqrt{\mu_0 \epsilon_0} \hat{e}_z \hat{e}_z \cdot \mathbf{E}$$

$$E_{z2} = A_3(e^{-q_1x}) + A_4(e^{q_1x}) + A_5(e^{-q_2x}) + A_6(e^{q_2x}) \tag{6}$$

$$H_{z2} = \frac{i\alpha_1}{\eta_t} (A_3(e^{-q_1x}) + A_4(e^{q_1x})) + \frac{i\alpha_2}{\eta_t} (A_5(e^{-q_2x}) + A_6(e^{q_2x})) \tag{7}$$

Other field components for region 2 can be derived from [32].

$$q_{1,2}^2 = \frac{\lambda^2}{2} \left[\frac{\mu_z}{\mu_t} + \frac{\epsilon_z}{\epsilon_t} \pm \sqrt{\left(\frac{\mu_z}{\mu_t} - \frac{\epsilon_z}{\epsilon_t}\right)^2 + \frac{4\varpi\xi^2\mu_z\epsilon_z}{\mu_t\epsilon_t}} \right] \tag{8}$$

where:

$$\lambda^2 = \beta^2 - \omega^2 \mu_t \epsilon_t \tag{9}$$

$$E_{z3} = A_7(e^{\alpha_{m1}x}) \tag{10}$$

$$H_{z3} = A_8(e^{\alpha_{m1}x}) \tag{11}$$

$$E_{y3} = \frac{i\omega\mu_0}{\alpha_{m1}} A_8 (e^{-\alpha_m x}) \tag{12}$$

$$H_{y3} = -\frac{i\omega\epsilon_0}{\alpha_m} A_7 (e^{-\alpha_m x}) \tag{13}$$

In above equations, $A_1, A_2, A_3, A_4, A_5, A_6, A_7,$ and A_8 are unknown amplitude constant. α_m is the wavenumber of region 1 and region 3, $\alpha_m = \sqrt{\beta^2 - k_0^2}$ and $k_0 = \omega\sqrt{\mu_0\epsilon_0}$.

To obtain the characteristic equation, the following boundary conditions are applied graphene-UAC-graphene waveguide structure.

$$\hat{x} \times [H_1 - H_2] = \sigma E \tag{14}$$

$$\hat{x} \times [E_1 - E_2] = 0 \tag{15}$$

where σ is the graphene conductivity taken from [6].

The following dispersion relation is obtained by using Eqs. 14 and 15.

$$\begin{bmatrix} 0 & \frac{\eta_l(\alpha_m+i\mu_0\sigma\omega)}{\alpha_m} & -\alpha_1 & -e^{2dq_1}\alpha_1 & -\alpha_2 & -e^{2dq_2}\alpha_2 & 0 & 0 \\ -\frac{\eta_l(\alpha_m\sigma+i\epsilon_0\omega)}{\alpha_m} & 0 & -k_l\alpha_1^2 & \frac{e^{2dq_1}k_l\alpha_1^2}{q_1} & -\frac{k_l\alpha_2^2}{q_2} & \frac{e^{2dq_2}k_l\alpha_2^2}{q_2} & 0 & 0 \\ 0 & -\frac{\mu_0\omega}{k_l\alpha_m} & -\frac{\alpha_1}{q_1} & \frac{e^{2dq_1}\alpha_1}{q_1} & -\frac{\alpha_2}{q_2} & \frac{e^{2dq_2}\alpha_2}{q_2} & 0 & 0 \\ i & 0 & -1 & -e^{2dq_1} & -1 & -e^{2dq_2} & 0 & 0 \\ 0 & 0 & e^{2dq_1}\alpha_1 & \alpha_1 & e^{2dq_2}\alpha_2 & \alpha_2 & 0 & -\frac{\eta_l(\alpha_m+i\mu_0\sigma\omega)}{\alpha_m} \\ 0 & 0 & \frac{e^{2dq_1}\alpha_1^2}{q_1} & -\frac{\alpha_1^2}{q_1} & \frac{e^{2dq_2}\alpha_2^2}{q_2} & -\frac{\alpha_2^2}{q_2} & -\frac{\eta_l(\alpha_m\sigma+i\epsilon_0\omega)}{k_l\alpha_m} & 0 \\ 0 & 0 & \frac{e^{2dq_1}k_l\alpha_1}{q_1} & -\frac{k_l\alpha_1}{q_1} & \frac{e^{2dq_2}k_l\alpha_2}{q_2} & -\frac{k_l\alpha_2}{q_2} & 0 & -\frac{\mu_0\omega}{\alpha_m} \\ 0 & 0 & \frac{q_1}{e^{2dq_1}} & 1 & \frac{q_2}{e^{2dq_2}} & 1 & -i & 0 \end{bmatrix} = 0 \tag{16}$$

influence of chirality and chemical potential on NPC versus operating frequency are shown in Fig. 2a and b respectively. In Fig. 2a, the variation in NPC under different chirality values are analyzed by using characteristic Eq. (16). Chirality values, i.e., $\xi = 0.2, \xi = 0.4,$ and $\xi = 0.6$ as indicated by black, red, and green peaks respectively. Obviously, operating frequency decreases with the increment of chirality, Furthermore, it is of peculiar of interest to note that NPC starts decreasing with the decrease of chirality value as reported in [33, 34]. Additionally, characteristic peaks level-off at lower operating frequencies mean at some higher frequencies unphysical region vanishes. Moreover, frequency band shows broadening as chirality increases from lower to higher value. The variation in NPC under different graphene’s chemical potentials are studied in Fig. 2b. Graphene chemical potential increases from, i.e., $\mu_c = 0.010 \text{ eV}, \mu_c = 0.020 \text{ eV},$ and $\mu_c = 0.030 \text{ eV},$ by keeping all other parameters which remains constant. Chemical potential can be tailored by gate voltage as reported in [6]. The operating frequency tends to increase with the increase of chemical potential.

Results

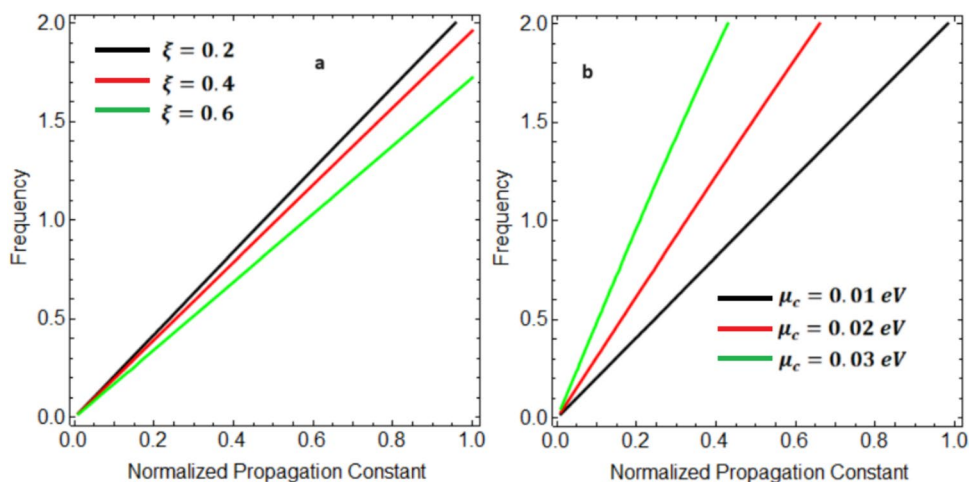
In this section, the plasmonic properties of graphene-UAC-graphene waveguide structure have been explored. The SPP characteristics of photon–plasmon coupling in UAC filled slab waveguide bounded by graphene layers are theoretically studied by using characteristic Eq. (16). To describe the anisotropy of uniaxial chiral medium, $\mu_t, \mu_z, \mu_1 = 1, \epsilon_t, \epsilon_z,$ and ξ are defined in next section. The normalized propagation constant (NPC) and attenuation versus operating frequency are analyzed for two types of UAC media.

Case I

In this case, we have set the UAC and graphene parameters as follows: $\mu_t = \mu_z = \mu_0, \mu_1 = 1, \epsilon_t = 0.2\epsilon_0, \epsilon_z = 0.3\epsilon_0, \xi = 0.3, \tau = 0.8 \text{ ps}, \mu_c = 0.010 \text{ eV},$ and $T = 300 \text{ K}.$ The

Additionally, the influence of chemical potential is more dominant at higher operating frequencies. Furthermore, NPC tends to decrease with the increment of chemical potential as reported in [6, 10, 35]. It is of peculiar interest to note that propagation band gap starts decreasing with increasing chemical potential. As chemical potential of graphene increases, energy levels shifted, resulting in shorter wavelengths and an increase in effective mass of charge carrier and consequently NPC decreases. The graphene’s chemical potential plays very crucial role in the field of plasmonics to fabricate graphene-based nano plasmonic devices. Figure 3a and b represents the NPC variations as a function of operating frequency for various values of relaxation time and chemical distance between the plates respectively. It can be observed from Fig. 3a that as the relaxation time of the graphene increases, the NPC decreases [11, 17, 33] and characteristic peaks are moving from low to high frequency region. Furthermore, as NPC increases, the operating frequency also increases.

Fig. 2 The variation in NPC at different values of chirality and chemical potential for graphene-UAC-graphene waveguide structure



Obviously, at higher frequencies, unphysical region vanishes. It is noteworthy that the graphene’s relaxation time of graphene depends on both the phenomenological scattering rate and the quality of the graphene itself [36]. When the relaxation time increases, the relaxation process is slowed down, thus resulting in a reduction in energy transfer and a slower propagation of SPP wave for proposed waveguide structure. To effectively study the geometrical parameter on the proposed waveguide structure, Fig. 3b is plotted under the different plate separation i , $d = 3\text{nm}$, $d = 4\text{nm}$, and $d = 5\text{nm}$. Tailoring separation distance between the plates will result in modifications to both the phase velocity dispersion and the group velocity dispersion of SPPs [37]. It is seen from figure that separation distance between the plates increases, NPC decreases and characteristic peaks are shifted from low to high frequency regime. Additionally, propagation band gap starts squeezing with the increment of separation distance between the plates in the proposed frequency range.

The variation in attenuation or propagation loss for different values of chemical potential and separation distance

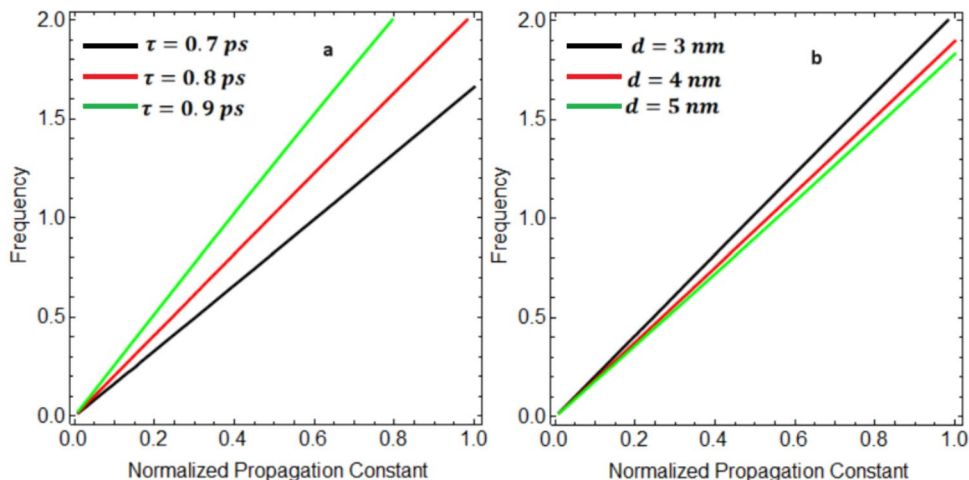
between graphene layers are depicted in Fig. 4a and b respectively. By varying graphene’s chemical potential and the separation distance between graphene layers, one can observe that the attenuation and operating frequency of the proposed waveguide structure can be modulated considerably.

Case II

In this case, we have set the UAC and graphene parameter values as follows: $\mu_t = \mu_z = \mu_0$, $\mu_1 = 1$, $\epsilon_t = -0.6\epsilon_0$, $\epsilon_z = 0.4\epsilon_0$, $\xi = 0.3$, $\tau = 0.8\text{ps}$, $\mu_c = 0.010\text{eV}$, and $T = 300\text{K}$. Figure 5a and b depict the numerical results of NPC versus operating frequency for the various values of chirality and chemical potentials.

One can observe from Fig. 5a that as chirality increases the operating frequency decreases, but propagation band gap broadened. Furthermore, highest NPC could be achieved at higher chirality values as reported in [28]. The slope of variation is smaller for lower chirality value. The pertaining values of chirality are strongly dependent on the nature and structure of the organic, inorganic, and biochemical

Fig. 3 The variation in NPC for various values of relaxation time and separation distance between graphene layers for graphene-UAC-graphene waveguide structure



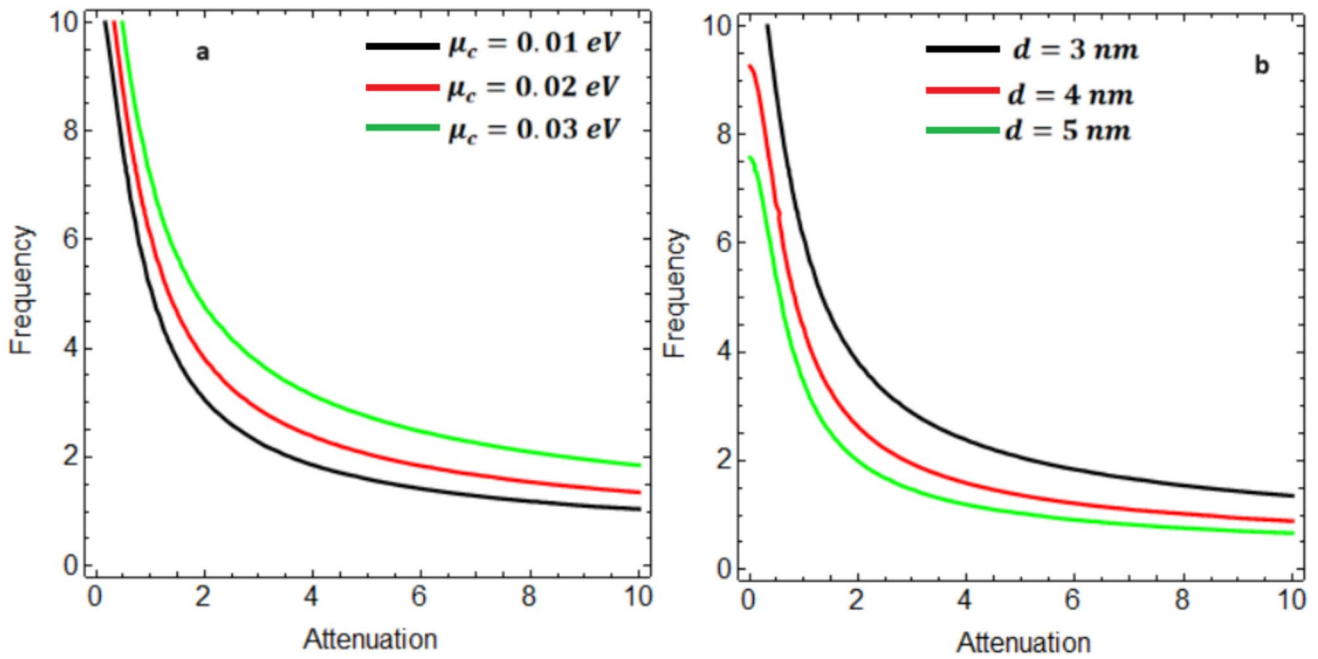


Fig. 4 The variation in attenuation at different values of chemical potential and separation distance between graphene layers for graphene-UAC-graphene waveguide structure

molecules as reported in [34–37]. To study the tunability of photon–plasmon coupling features of proposed waveguide structure by varying chemical potentials, i.e., $\mu_c = 0.010$ eV, $\mu_c = 0.020$ eV, and $\mu_c = 0.030$ eV kept, all other parameter values remain constant; Fig. 5b is analyzed. It is seen from Fig. 5b that NPC increases by decreasing graphene’s chemical potential [38, 39] and unphysical region occurs at some lower frequency that has no practical importance in optics community as reported in [40]. The former tunability trait suggests that SPP wave can be engineered by graphene’s chemical potential. Increasing chemical potential increases Fermi level, which in turn increases carrier density. Increasing carrier density results in a decrease in propagation

constant. Figure 6a illustrates the influence of relaxation time on NPC as the function of operating frequency along graphene-uniaxial chiral-graphene waveguide structure.

As relaxation time increases, operating frequency also increases, but NPC tends to decrease as reported in [39]. Furthermore, it is important to note that characteristic peaks are level-off at some lower frequencies that exhibit unphysical region. It is vital to note that, as relaxation time increases, frequency band starts squeezing and characteristic peaks are shifted towards high frequency region. As graphene’s relaxation time increases, its quasiparticles acquire less energy and momentum, which results in a decrease in the normalized propagation constant. The separation

Fig. 5 The variation in NPC at different values of chirality and chemical potential for graphene-UAC-graphene waveguide structure

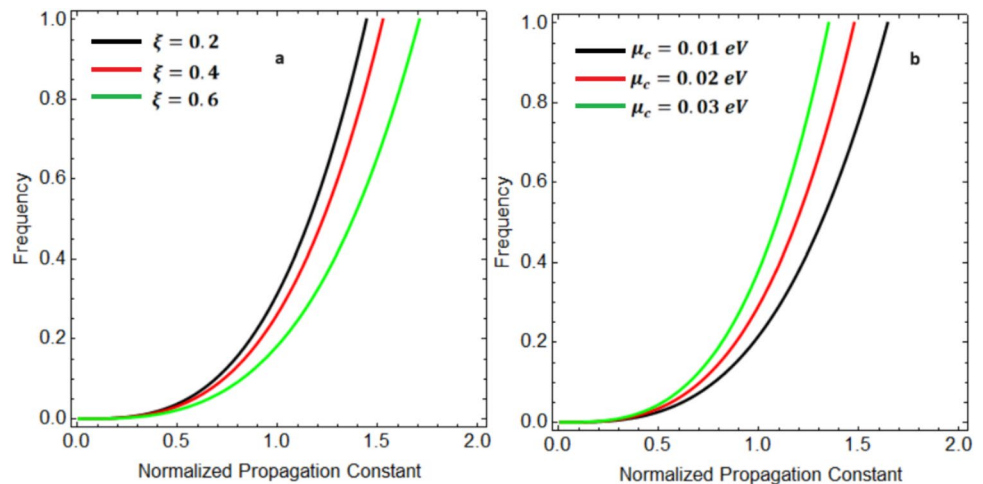
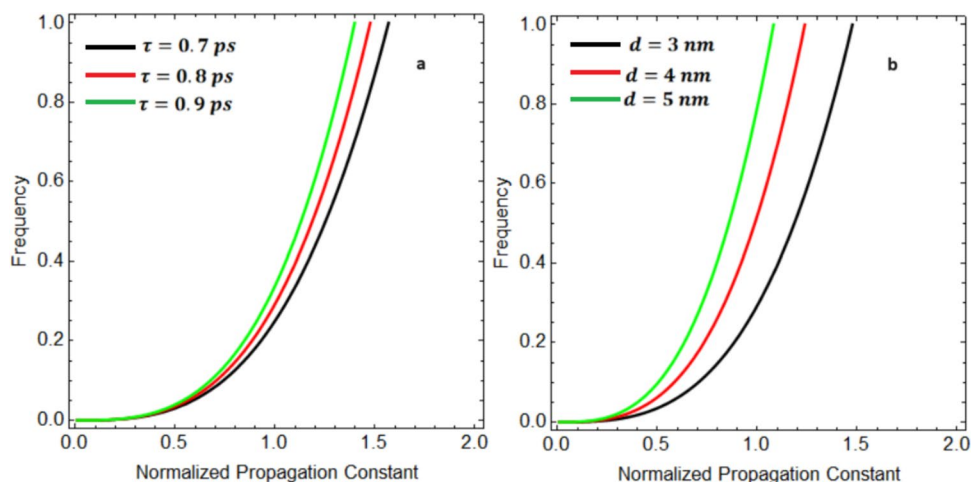


Fig. 6 The variation in NPC for various values of relaxation time and separation distance between graphene layers for graphene-UAC-graphene waveguide structure



distance between graphene layers has a strongly effect the characteristics of SPPs due to the coupling effect [10]. The variation in NPC under the different values of separation distance between graphene layers is illustrated in Fig. 6b. As separation distance between the graphene layers is changed, the phase velocity dispersion and the group velocity dispersion of the SPPs changed, as well as the field confinement

making it a highly promising platform for sensing applications. The influence of chemical potential and separation distance between graphene layers are analyzed in Fig. 7a and b respectively. Based on the above analysis, it is shown that graphene’s chemical potential and separation distance between graphene layers can significantly influence attenuation and operating frequency of the proposed waveguide.

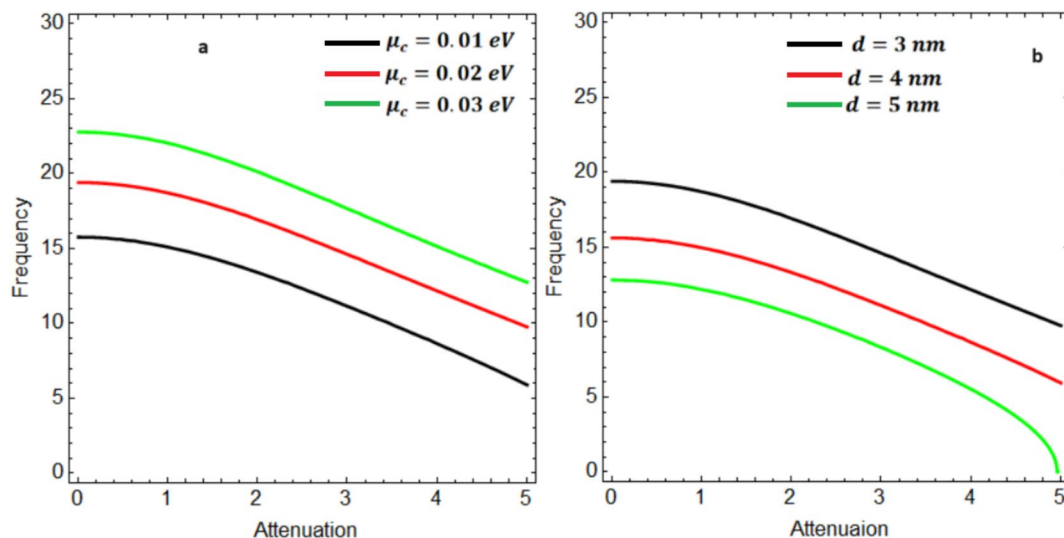


Fig. 7 The variation in attenuation at different values of chemical potential and separation distance between graphene layers for graphene-UAC-graphene waveguide structure

Conclusion

We have illustrated the plasmonic characteristics of photon–plasmon coupling in UAC sandwiched waveguide structure bounded by graphene layers. Graphene conductivity is modeled with Kubo formalism and boundary conditions are employed to obtain the characteristics equation. The characteristic equation is plotted to explore the behavior of proposed waveguide structure. We found that chirality, chemical potential, relaxation time, and separation distance between graphene layers can be used to modulate the SPPs. Furthermore, chemical potential and separation distance between graphene layers can also be used to tune the SPPs. This study can be used to fabricate graphene-based nanophotonic devices in the optics sector.

Acknowledgements The authors extend their appreciation to Taif University, Saudi Arabia, for supporting this work through project number (TU-DSPP-2024-01).

Author Contribution The authors confirm their contribution to the manuscript as follows: Laiba and Ahmed Mahal wrote the main manuscript. Laiba, Hussein H. Abdulghani, Raad A. Khamis, Yazeed M. Asiri, Mohammed A. Amin, Majid S. Jabir, and Hasan Majdi derived analytical expressions. Fahad M. Almutairi, Adel Ashour, and Mohamed Shaban wrote the result and discussion. Authors Laiba and Ahmed Mahal were also encouraged and completely supervised during preparation of the manuscript. All authors reviewed the manuscript before submission.

Funding This research was funded by Taif University, Saudi Arabia, Project No. TU-DSPP-2024-01.

Data Availability All the associated data is provided within the framework of the article.

Declarations

Ethical Approval Not applicable.

Competing Interests The authors declare no competing interests.

References

- Fang Y, Sun M (2015) Nanoplasmonic waveguides towards applications in integrated nanophotonic circuits. *Light Sci Appl* 4(6):e294–e294
- Azam M et al (2024) Dispersion characteristics of surface plasmon polaritons (SPPs) in graphene–chiral–graphene waveguide. *Waves in Random and Complex Media* 34(1):134–145
- Kleine-Ostmann T, Nagatsuma T (2011) A review on terahertz communications research. *J Infrared Millim Terahertz Waves* 32:143–171
- Pickwell E, Wallace V (2006) Biomedical applications of terahertz technology. *J Phys D: Appl Phys* 39(17):R301
- Tonouchi M (2007) Cutting-edge terahertz technology. *Nature photonics* 1(2):97–105
- Umair M et al. (2023) Plasmonic Characteristics of Monolayer Graphene in Anisotropic Plasma Dielectric. *Plasmonics* p. 1-7
- Umair M et al. (2023) Hybrid Plasmon Modes at Chiroferrite-Graphene Interface. *Plasmonics* p. 1-7
- Pendry J, Martin-Moreno L, Garcia-Vidal F (2004) Mimicking surface plasmons with structured surfaces. *Science* 305(5685):547–848
- Ulrich R, Tacke M (1973) Submillimeter waveguiding on periodic metal structure. *Applied Physics Letters* 22(5):251–253
- Zhao T et al (2016) Plasmon modes of circular cylindrical double-layer graphene. *Optics express* 24(18):20461–20471
- Ogawa S, Fukushima S, Shimatani M (2020) Graphene plasmonics in sensor applications: A review. *Sensors* 20(12):3563
- Komjani Hosseini S, N, (2016) Comparative analysis of graphene-integrated slab waveguides for terahertz plasmonics. *Photonics and Nanostructures-Fundamentals and Applications* 20:59–67
- Yaqoob M et al (2018) Hybrid surface plasmon polariton wave generation and modulation by chiral-graphene-metal (CGM) structure. *Sci rep* 8(1):18029
- Novoselov KS et al (2007) Room-temperature quantum Hall effect in graphene. *Science* 315(5817):1379–1379
- Novoselov KS et al (2006) Unconventional quantum Hall effect and Berry's phase of 2π in bilayer graphene. *Nat phys* 2(3):177–180
- Bonaccorso F et al (2010) Graphene photonics and optoelectronics. *Nat photonics* 4(9):611–622
- Nair RR (2008) Fine structure constant defines visual transparency of graphene. *Science* 320(5881):1308–1308
- Singh V et al (2011) Graphene based materials: past, present and future. *Prog mater sci* 56(8):1178–1271
- Heydari MB, Samiei MHV (2018) Plasmonic graphene waveguides: A literature review. *arXiv preprint arXiv:1809.09937*
- Azam M et al (2021) Electromagnetic energy surface modes in metamaterial-filled bi-layer graphene structures. *Plasmonics* 16:1175–1194
- Gric T (2021) Surface plasmons in metamaterial heterostructures. *Waves in Random and Complex Media* 31(6):1246–1257
- Ioannidis T, Gric T, Rafailov E (2020) Surface plasmon polariton waves propagation at the boundary of graphene based metamaterial and corrugated metal in THz range. *Opt quantum electron* 52:1–12
- Umair M et al (2020) Characteristics of surface plasmon polaritons in magnetized plasma film walled by two graphene layers. *Journal of Nanoelectronics and Optoelectronics* 15(5):574–579
- Umair M et al (2023) Plasmonic modes of metallic slab in anisotropic plasma environment. *Plasmonics* 18(5):1857–1864
- You B, et al. (2014) Terahertz plasmonic waveguide sensing based on metal rod array structures. in *Terahertz, RF, Millimeter, and Submillimeter-Wave Technology and Applications VII. SPIE*
- Mi G, Van V (2014) Characteristics of surface plasmon polaritons at a chiral–metal interface. *Optics letters* 39(7):2028–2031
- Umair M et al (2021) Dispersion characteristics of hybrid surface waves at chiral-plasma interface. *J Electromagn Waves Appl* 35(2):150–162
- Umair M et al (2024) Dyakonov waves generation at uniaxial chiral-plasma interface. *Optics Express* 32(3):4376–4386
- Yaqoob MZ et al (2019) Characteristics of light–plasmon coupling on chiral–graphene interface. *JOSA B* 36(1):90–95
- Xu J-P (1996) Propagation characteristics of a circular waveguide filled with a chiroferrite medium. *Int j infrared millim waves* 17:193–203
- Heydari MB, Samiei MHV, (2021) TM-polarized Surface Plasmon Polaritons in Nonlinear Multi-layer Graphene-Based Waveguides: An Analytical Study. *arXiv preprint arXiv:2101.02536*
- Gonçalves PAD, Peres NM (2016) An introduction to graphene plasmonics. *World Scientific*
- Zhang X et al (2020) Terahertz surface plasmonic waves: a review. *Advanced Photonics* 2(1):014001–014001

34. Berova N et al (2011) *Comprehensive Chiroptical Spectroscopy, Volume 1: Instrumentation, Methodologies, and Theoretical Simulations*. Vol. 1. John Wiley & Sons
35. Hentschel M et al (2017) Chiral plasmonics. *Sci adv* 3(5):e1602735
36. Wu T, Kessler J, Bouř P (2016) Chiral sensing of amino acids and proteins chelating with Eu III complexes by Raman optical activity spectroscopy. *Phys Chem Chem Phys* 18(34):23803–23811
37. Yoo S, Park Q-H (2019) Metamaterials and chiral sensing: a review of fundamentals and applications. *Nanophotonics* 8(2):249–261
38. Gu X, Lin I-T, Liu J-M (2013) Extremely confined terahertz surface plasmon-polaritons in graphene-metal structures. *Appl Phys Lett* 103(7)
39. Ghaffar A et al (2022) Dispersion characteristics of surface plasmon polaritons in a graphene–plasma–graphene waveguide structure. *Can J Phys* 100(2):123–128
40. Umair M et al (2023) Light Plasmon Coupling in Planar Chiro-plasma-Graphene Waveguides. *Plasmonics* 18(3):1029–1035

Publisher's Note Springer Nature remains neutral with regard to jurisdictional claims in published maps and institutional affiliations.

Springer Nature or its licensor (e.g. a society or other partner) holds exclusive rights to this article under a publishing agreement with the author(s) or other rightsholder(s); author self-archiving of the accepted manuscript version of this article is solely governed by the terms of such publishing agreement and applicable law.